

# Effect of Mo content on glass forming ability and crystallization behavior of Fe-based alloy prepared by atmospheric plasma spraying

Guanchong Wang<sup>a</sup>, Lajun Feng<sup>a,b,\*</sup>, Wenning Shen<sup>a,b</sup>, Zheng Liu<sup>a</sup>

<sup>a</sup> School of Materials Science and Engineering, Xi'an University of Technology, No. 5 South Jinhua Road, Xi'an 710048, China

<sup>b</sup> Key Lab. of Corrosion and Protection of Shaanxi Province, Xi'an University of Technology, No. 5 South Jinhua Road, Xi'an 710048, China

## ARTICLE INFO

### Keywords:

Fe-based amorphous alloy  
Crystallization behavior  
Mo addition

## ABSTRACT

The preparation of Fe-based amorphous alloys has the problems of high cost due to the use of high purity raw materials and low production efficiency of copper mould suction casting. Herein, Fe<sub>75.5-x</sub>Cr<sub>4</sub>Si<sub>3.5</sub>P<sub>9.5</sub>B<sub>7.5</sub>Mo<sub>x</sub> (x = 0, 1, 3, 5, 7) alloys with a thickness of 100–300 μm were prepared by atmospheric plasma spraying method using industrial raw materials and commercial pure materials as starting materials. The effects of Mo contents on the glass forming ability and crystallization behavior were analyzed. Microstructure and crystallization behavior of as-prepared alloys were characterized by X-ray diffraction (XRD), transmission electron microscopy (TEM) and differential scanning calorimeter (DSC). The plasma spraying prepared Fe<sub>75.5-x</sub>Cr<sub>4</sub>Si<sub>3.5</sub>P<sub>9.5</sub>B<sub>7.5</sub>Mo<sub>x</sub> with 0 and 5 at% of Mo exhibited fully amorphous alloy features. When Mo content was 5 at %, the crystallization temperature of amorphous alloy increased and the crystallization process changed from one step (amorphous → α-Fe(Si) + Fe<sub>3</sub>B + Fe<sub>2</sub>P) to two steps (amorphous → α-Fe(Mo, Si) → α-Fe(Mo, Si) + Fe<sub>3</sub>B + Fe<sub>2</sub>P), in which the apparent activation energy of crystallization increased from 475 kJ mol<sup>-1</sup> to 542 kJ mol<sup>-1</sup> and 546 kJ mol<sup>-1</sup>. It could be concluded that the enhanced glass forming ability and thermal stability are attributed to the suppression of heterogeneous nucleation by addition optimum amount of Mo. It would provide a basis for the practical application of Fe-based amorphous alloys.

## Introduction

Fe-based amorphous alloys have attractive properties, such as high strength, soft magnetic properties and good corrosion resistance, which have potential applications in the fields of transformers and sensors [1–4]. However, their practical applications have been limited due to their poor glass forming ability [5]. A large number of studies have shown that the glass forming ability of Fe-based alloy can be enhanced by adding proper elements, which exhibits excellent properties [6]. For example, the addition of element P to Fe-Si-B alloy improved the glass forming ability and increased its saturation magnetization [7]. The addition of element Cr into Fe-Mo-Ga-P-C-B-Si alloy improved its glass formation ability and corrosion resistance [8]. The addition of element Co had improved the glass forming ability of Fe-Cr-Mo-C-B-Y alloy and increased its fracture strength [9]. However, the high cost for the improvement of Fe-based alloys' glass forming ability has limited their commercial applications due to the use of highly pure raw materials.

Some research has tried to fabricate cost-effective Fe-based amorphous alloys by copper mould suction casting method, using industrial raw materials and industrial pure metals as the precursor materials. Li

*et al.* had successfully prepared Fe-based bulk amorphous alloy in Fe-C-Si-B-P-Cr-Al-Mo system by copper mould suction casting method, using industrial raw materials and commercial metals as precursors [10]. Subsequently, small amounts of B and Co had systematically substituted Fe to enhance the glass forming ability [11] and magnetic properties [12]. Wang *et al.* [13] prepared amorphous alloy in Fe-C-Si-B-P-Cr-Al-Mo system by copper mould suction casting method and improved its corrosion resistance by adjusting the content of element Cr. Amorphous alloy with excellent properties has been successfully prepared by copper mould suction casting method, using cost-effective industrial raw materials as precursors. However, under the strictly working conditions of inert atmosphere, it can only work intermittently, resulting in the low production efficiency.

Atmosphere plasma spraying method has the advantages of consecutive operation, low cost, simplicity, and flexibility [14,15]. Moreover, it can provide higher undercooling than that of copper mode casting, favoring fabricating amorphous phase, especially for the alloy systems with a lower glass forming ability [16]. We have tried to fabricate Fe-C-Si-B-P-Cr-Al-Mo amorphous alloy using industrial raw materials and industrial pure metals by atmosphere plasma spraying. It

\* Corresponding author at: School of Materials Science and Engineering, Xi'an University of Technology, No. 5 South Jinhua Road, Xi'an 710048, China.

E-mail address: [fenglajun@xaut.edu.cn](mailto:fenglajun@xaut.edu.cn) (L. Feng).

<https://doi.org/10.1016/j.rinp.2019.102512>

Received 1 April 2019; Received in revised form 5 July 2019; Accepted 6 July 2019

Available online 15 July 2019

2211-3797/ © 2019 The Authors. Published by Elsevier B.V. This is an open access article under the CC BY-NC-ND license (<http://creativecommons.org/licenses/by-nc-nd/4.0/>).

was found that the segregation of carbon with a high melting point and the oxidation of aluminum occurred during the spraying process. The segregated carbon and oxidized aluminum became heterogeneous nucleated points, deteriorating the glass formation ability of the alloy. Therefore, the elements of carbon and aluminum were removed in this alloy and remaining Fe-Cr-Si-P-B-Mo system was used as the basic alloy system. The contents of elements Cr, Si, P, B, Mo have an effect on the glass formation ability of Fe-based alloys. However, Cr, Si, P and B were introduced in the form of industrial raw materials contained various impurities. It is difficult to systematically investigate these elements' effects on the glass forming ability. Thus, the amorphous alloy in Fe-Cr-P-Si-B was prepared by atmosphere plasma spraying method and the effects of Mo content on glass forming ability and crystallization behavior were studied.

## Experimental

### Experiment materials

Industrial pure iron, industrial silicon iron, industrial boron iron, industrial phosphorus iron, industrial ferrochrome and commercial pure Mo were used as raw materials without further purification. The specific components are listed in Table 1.

### Preparation of master alloy for spraying

The master alloy for spraying was prepared by smelting process. First, raw materials were mixed in acetone solution and ultrasonic cleaned for 20 min. The ferromagnetic alloy bar with a nominal composition of  $\text{Fe}_{75.5-x}\text{Cr}_4\text{Si}_{3.5}\text{P}_{9.5}\text{B}_{7.5}\text{Mo}_x$  ( $x = 0, 1, 3, 5, 7$ ) was smelted in DHL-400 vacuum arc furnace with electromagnetic stirring to ensure homogeneous for four times. Thereafter, the prepared alloy ingot was cut into long bar with a section of  $2\text{ mm} \times 2\text{ mm}$  by wire electrical discharge machining and then ultrasonic cleaned in kerosene and ethanol solution for further use.

### Preparation of amorphous alloy in FeCrSiBPMo system

Amorphous alloy in FeCrSiBPMo system was prepared by using GP-80 atmospheric plasma spraying equipment. The alloy bar under the flame of the nozzle was sprayed onto a copperplate ( $500\text{ mm} \times 500\text{ mm} \times 5\text{ mm}$ ) and flattened into alloy sheets with a thickness of  $100\text{--}300\text{ }\mu\text{m}$ . The process parameters of spraying are as follows, spraying voltage of 55 V, spraying current of 600 A, distance between the bar and the nozzle of 3 mm, rod feeding rate of  $50\text{ mm}\cdot\text{min}^{-1}$ , spraying distance of 300 mm, the argon pressure and flow rate of 0.85 MPa and  $1600\text{ L}\cdot\text{h}^{-1}$ , the hydrogen pressure and flow rate of 0.32 MPa and  $300\text{ L}\cdot\text{h}^{-1}$ .

### Characterization

The phase composition and crystal structure of the product were analyzed by powder X-ray diffractometer (XRD-7000) with a monochromatic  $\text{CuK}\alpha$  radiation. The diffraction angle  $2\theta$  ranged from  $20^\circ$  to  $80^\circ$ . The scanning velocity was  $8^\circ\text{ min}^{-1}$ . The tube voltage and tube

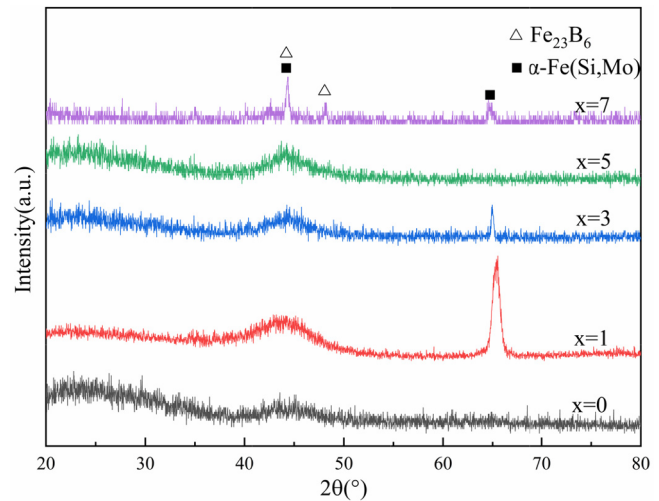


Fig. 1. XRD patterns of  $\text{Fe}_{75.5-x}\text{Cr}_4\text{Si}_{3.5}\text{P}_{9.5}\text{B}_{7.5}\text{Mo}_x$  ( $x = 0, 1, 3, 5, 7$ ) alloys obtained by plasma spraying.

current were 40 V and 40 mA, respectively.

The diffraction pattern of the product was observed by transmission electron microscope (JEM-3010). The acceleration voltage was 200 kV.

The crystallization process of the product was analyzed by NETZSCH STA 449F3 differential calorimeter. During the test, the Ar gas (99.9%) was used to protect the product and the argon gas flow rate was  $100\text{ mL}\cdot\text{min}^{-1}$ .

## Results and discussion

### Microstructure of $\text{Fe}_{75.5-x}\text{Cr}_4\text{Si}_{3.5}\text{P}_{9.5}\text{B}_{7.5}\text{Mo}_x$ alloy

Fig. 1 shows the XRD patterns of  $\text{Fe}_{75.5-x}\text{Cr}_4\text{Si}_{3.5}\text{P}_{9.5}\text{B}_{7.5}\text{Mo}_x$  ( $x = 0, 1, 3, 5, 7$ ) alloys obtained by plasma spraying. Only one broad diffuse scattering peak at  $40^\circ\text{--}50^\circ$  was observed for the alloy prepared by plasma spraying of  $\text{Fe}_{75.5}\text{Cr}_4\text{Si}_{3.5}\text{P}_{9.5}\text{B}_{7.5}$  alloy. This indicates that amorphous alloy has been obtained. After adding element Mo, the broad diffraction peak at  $40^\circ\text{--}50^\circ$  appeared in  $\text{Fe}_{75.5-x}\text{Cr}_4\text{Si}_{3.5}\text{P}_{9.5}\text{B}_{7.5}\text{Mo}_x$  ( $x = 1, 3, 5$ ) alloys, indicating the existence of amorphous phase in spraying products. In addition, a sharp diffraction peak at  $65.3^\circ$  appeared in spraying  $\text{Fe}_{75.5-x}\text{Cr}_4\text{Si}_{3.5}\text{P}_{9.5}\text{B}_{7.5}\text{Mo}_x$  ( $x = 1, 3$ ) alloys, corresponding to (2 0 0) crystal plane of  $\alpha\text{-Fe}(\text{Mo}, \text{Si})$ . With the increase of Mo content, the intensity of (2 0 0) peak of  $\alpha\text{-Fe}(\text{Mo}, \text{Si})$  decreased and became undetectable in  $\text{Fe}_{70.5}\text{Cr}_4\text{Si}_{3.5}\text{P}_{9.5}\text{B}_{7.5}\text{Mo}_5$  system. When the content of Mo increased to 7 at%, the broad diffuse scattering peak vanished and new diffraction peaks appeared at  $44.6^\circ$ ,  $48.1^\circ$  and  $65.0^\circ$ , corresponding to  $\alpha\text{-Fe}(\text{Mo}, \text{Si})$  and  $\text{Fe}_{23}\text{B}_6$  [17]. These results indicate that the content of element Mo had a great influence on the glass forming ability of  $\text{Fe}_{75.5-x}\text{Cr}_4\text{Si}_{3.5}\text{P}_{9.5}\text{B}_{7.5}\text{Mo}_x$  ( $x = 0, 1, 3, 5, 7$ ) alloys. The influential action is manifested in two aspects. On one hand, the relative radius difference and enthalpy of mixing between Mo and Fe, Cr, Si, P, B atoms are 10.23% and  $-2\text{ kJ}\cdot\text{mol}^{-1}$ , 10.23% and  $0\text{ kJ}\cdot\text{mol}^{-1}$ , 4.48% and  $-35\text{ kJ}\cdot\text{mol}^{-1}$ , 7.09% and  $-53.5\text{ kJ}\cdot\text{mol}^{-1}$ ,

Table 1

Components of raw materials (wt%).

	Fe	Si	Mn	P	S	C	B	Cr
industrial pure iron	99.787	0.012	0.13	0.007	0.006	0.002	0	0.030
industrial silicon iron	23.982	75.43	0.30	0.028	0.019	0.088	0	0.24
industrial boron iron	80.27	0.42	0	0.026	0.002	0.36	17.4	0
industrial phosphorus iron	74.06	0.92	0.86	24.08	0.03	0.05	0	0
industrial ferrochrome	36.651	0.025	0	0.027	0.38	0.027	0	62.89
commercial pure Mo > 99%								

47.37% and  $-34 \text{ kJ} \cdot \text{mol}^{-1}$ , respectively [18]. Since the negative enthalpy of mixing between Mo and Si, Mo and P, Mo and B is larger, the atomic mobility in the liquid alloy is decreased. Thus, the addition of Mo could hinder the formation of  $\alpha\text{-Fe}(\text{Mo}, \text{Si})$  primary phase and improve the glass formation ability of Fe-based alloy [10]. On the other hand, Mo has similar atomic radius and electronegativity with Fe [19], favoring the formation of solid solutions [20,21]. The glass formation ability of this alloy in FeCrSiPBMo system would be extremely low due to the large solubility of element Mo in  $\alpha\text{-Fe}(\text{Mo}, \text{Si})$  crystalline phases and no requirement of long-range atomic rearrangements. When 1 at% Mo was added into the alloy, it preferred to form solid solution. Thus, the glass formation ability was greatly decreased and  $\alpha\text{-Fe}(\text{Mo}, \text{Si})$  crystalline phases formed. As the content of Mo increased, the glass formation ability was improved due to the greater negative enthalpy of mixing. It would be beneficial to form amorphous alloy. So the intensity of (200) peak decreased. However, when the Mo content was larger than 5 at%, the excessive Mo resulted in the decrease of Fe atomic concentration, leading to the variation of the original crystallization behavior, and deteriorating the glass formation ability of the alloy. Thus, there is a diversely optimal addition of Mo with best glass forming ability for various Fe-based alloys, such as 6 at% in FePCMo alloy [22], 2 at% in FeSiBPMo alloy [23] and 12 at% in FeCBrWMo alloy [24].

Fig. 2 shows the TEM bright-field images with selected area diffraction patterns (inset) of  $\text{Fe}_{75.5-x}\text{Cr}_4\text{Si}_{3.5}\text{P}_{9.5}\text{B}_{7.5}\text{Mo}_x$  ( $x = 0, 5$ ) alloys obtained by plasma spraying method. The TEM bright-field images of the two products both revealed a uniform contrast, and the selected area electron diffraction patterns both exhibited diffuse halo rings. These results proved the formation of fully amorphous alloy.

#### Crystallization behavior

Fig. 3 shows DSC curves of plasma spraying prepared  $\text{Fe}_{75.5-x}\text{Cr}_4\text{Si}_{3.5}\text{P}_{9.5}\text{B}_{7.5}\text{Mo}_x$  ( $x = 0, 3, 5$ ) alloys. There is only one crystallization exothermic peak in prepared  $\text{Fe}_{75.5}\text{Cr}_4\text{Si}_{3.5}\text{P}_{9.5}\text{B}_{7.5}$  alloy without the addition of Mo. After the addition of Mo, two exothermic peaks emerged, indicating the change of the crystallization behavior. The crystallization behavior of Fe-based amorphous alloy usually contains a single or multiple stages, where the first exothermic peak is  $\alpha\text{-Fe}$  crystallization and the subsequent exothermic peak is Fe-B crystallization [25]. The onset crystallization temperature and peak

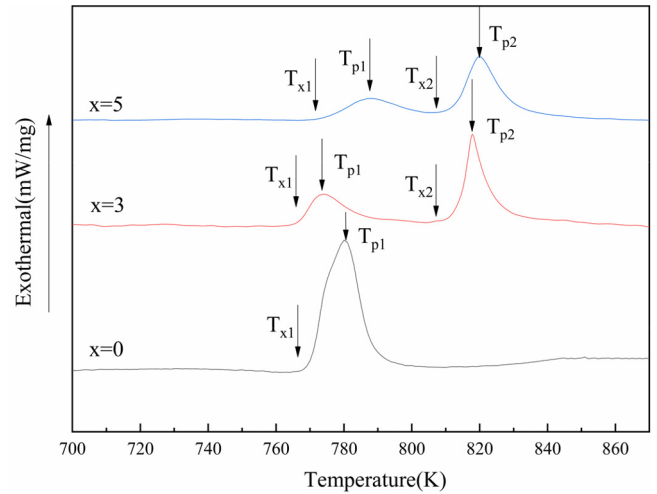


Fig. 3. DSC curve of  $\text{Fe}_{75.5-x}\text{Cr}_4\text{Si}_{3.5}\text{P}_{9.5}\text{B}_{7.5}\text{Mo}_x$  ( $x = 0, 3, 5$ ) alloys obtained by plasma spraying.

Table 2

Characteristic temperatures of  $\text{Fe}_{75.5-x}\text{Cr}_4\text{Si}_{3.5}\text{P}_{9.5}\text{B}_{7.5}\text{Mo}_x$  ( $x = 0, 3, 5$ ) alloys obtained from DSC curves.

Samples	$T_{x1}(\text{K})$	$T_{p1}(\text{K})$	$T_{x2}(\text{K})$	$T_{p2}(\text{K})$
$x = 0$	768	781		
$x = 3$	768	774	807	818
$x = 5$	772	787	807	820

temperature of first exothermic peak were set as  $T_{x1}$  and  $T_{p1}$  and those of second exothermic peaks were set as  $T_{x2}$  and  $T_{p2}$ , respectively. Detail temperatures are shown in Table 2. As shown in Table 2,  $T_{x1}$ ,  $T_{x2}$ ,  $T_{p1}$  and  $T_{p2}$  were higher with the addition of Mo. These results indicated that thermal stability of amorphous alloy could be improved by the addition of Mo, and the precipitation of  $\alpha\text{-Fe}$  and Fe-B phase was also inhibited in some extent. But there is an appreciable decline of  $T_{p1}$  in plasma spraying prepared product with the addition of 3 at% Mo. It might be due to the existence of crystal phase in plasma spraying prepared product. To eliminate the interference of crystal phase, the crystallization behavior of  $\text{Fe}_{75.5-x}\text{Cr}_4\text{Si}_{3.5}\text{P}_{9.5}\text{B}_{7.5}\text{Mo}_x$  ( $x = 0, 5$ ) alloys

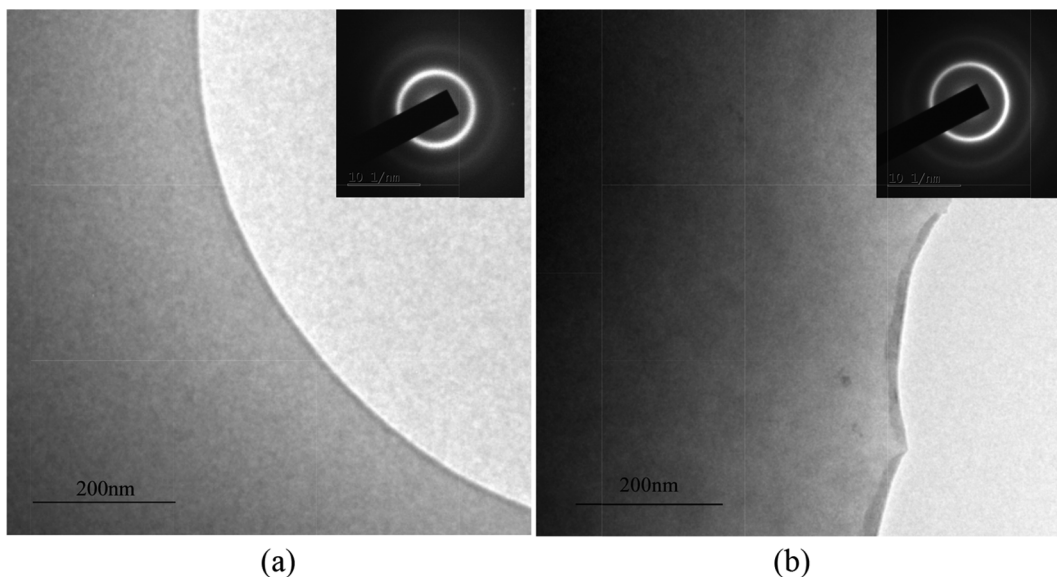


Fig. 2. TEM images of  $\text{Fe}_{75.5-x}\text{Cr}_4\text{Si}_{3.5}\text{P}_{9.5}\text{B}_{7.5}\text{Mo}_x$  ( $x = 0, 5$ ) alloys obtained by plasma spraying (a)  $x = 0$  (b)  $x = 5$ .

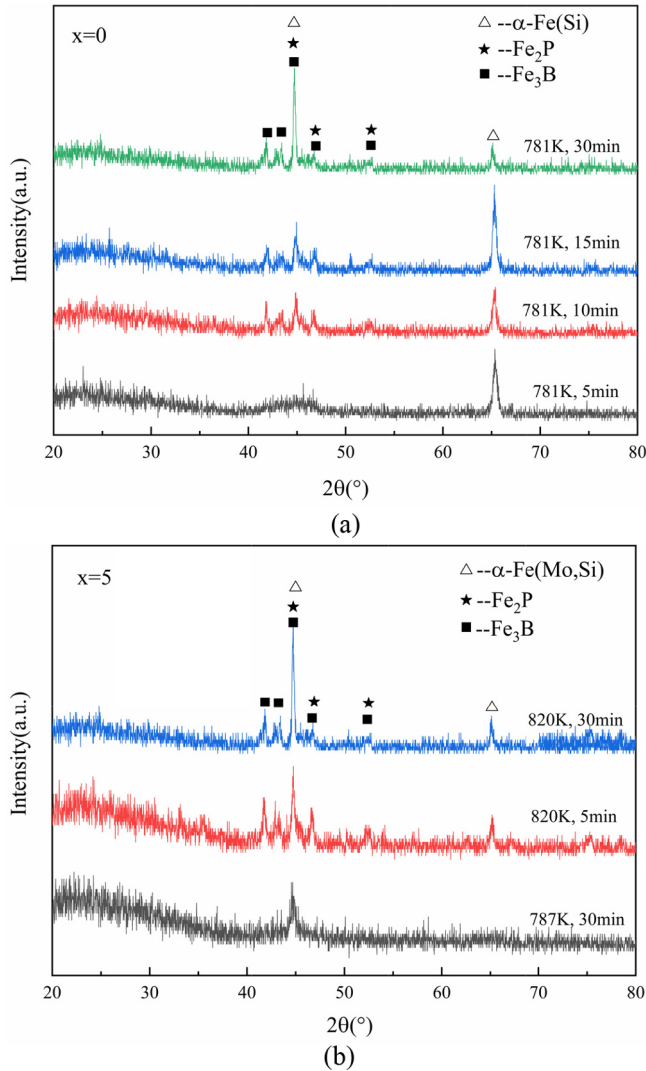


Fig. 4. XRD patterns of the  $\text{Fe}_{75.5-x}\text{Cr}_4\text{Si}_{3.5}\text{P}_{9.5}\text{B}_{7.5}\text{Mo}_x$  ( $x = 0, 5$ ) alloys after annealed at different temperatures (a)  $x = 0$  (b)  $x = 5$ .

with fully amorphous phase were investigated.

Fig. 4 presents XRD patterns of plasma spraying prepared  $\text{Fe}_{75.5-x}\text{Cr}_4\text{Si}_{3.5}\text{P}_{9.5}\text{B}_{7.5}\text{Mo}_x$  ( $x = 0, 5$ ) amorphous alloys annealed at  $T_{p1}$  and  $T_{p2}$  temperatures at the heating rate of  $10 \text{ K} \cdot \text{min}^{-1}$  respectively. The alloy without the addition of Mo exhibited a diffraction peak of  $\alpha\text{-Fe}(\text{Si})$  phase after annealed at  $781 \text{ K}$  ( $T_{p1}$ ) for 5 min. After annealed for 10 min, obvious diffraction peaks of  $\alpha\text{-Fe}(\text{Si})$ ,  $\text{Fe}_2\text{P}$  and  $\text{Fe}_3\text{B}$  phases were observed. These results indicate that the exothermic peak of prepared  $\text{Fe}_{75.5}\text{Cr}_4\text{Si}_{3.5}\text{P}_{9.5}\text{B}_{7.5}$  alloy corresponded to the crystallization of  $\alpha\text{-Fe}(\text{Si})$ ,  $\text{Fe}_2\text{P}$  and  $\text{Fe}_3\text{B}$  phases. As for prepared  $\text{Fe}_{70.5}\text{Cr}_4\text{Si}_{3.5}\text{P}_{9.5}\text{B}_{7.5}\text{Mo}_5$  alloy after annealed at  $787 \text{ K}$  ( $T_{p1}$ ) for 30 min, only the diffraction peak of  $\alpha\text{-Fe}(\text{Mo}, \text{Si})$  phase was observed, suggesting that the first exothermic peak of prepared  $\text{Fe}_{70.5}\text{Cr}_4\text{Si}_{3.5}\text{P}_{9.5}\text{B}_{7.5}\text{Mo}_5$  alloy corresponded to the crystallization of  $\alpha\text{-Fe}(\text{Mo}, \text{Si})$  phase. However, the diffraction peaks of  $\alpha\text{-Fe}(\text{Mo}, \text{Si})$ ,  $\text{Fe}_2\text{P}$  and  $\text{Fe}_3\text{B}$  phases appeared simultaneously after annealing at  $830 \text{ K}$  ( $T_{p2}$ ) for 5 min. As the annealing time extended to 30 min, the intensity of diffraction peaks were enhanced without new diffraction peak, indicating the completion of the crystallization. These results suggest that the addition of 5 at% Mo could promote the crystal phase separation of  $\alpha\text{-Fe}(\text{Si}, \text{Mo})$ ,  $\text{Fe}_3\text{B}$  and  $\text{Fe}_2\text{P}$ .

The transformation of crystallization behavior of  $\text{Fe}_{70.5}\text{Cr}_4\text{Si}_{3.5}\text{P}_{9.5}\text{B}_{7.5}\text{Mo}_5$  might be caused by several factors. First, the negative enthalpy of mixing between Mo and P, Mo and B are larger than that between Fe and P, Fe and B. With the addition of Mo,

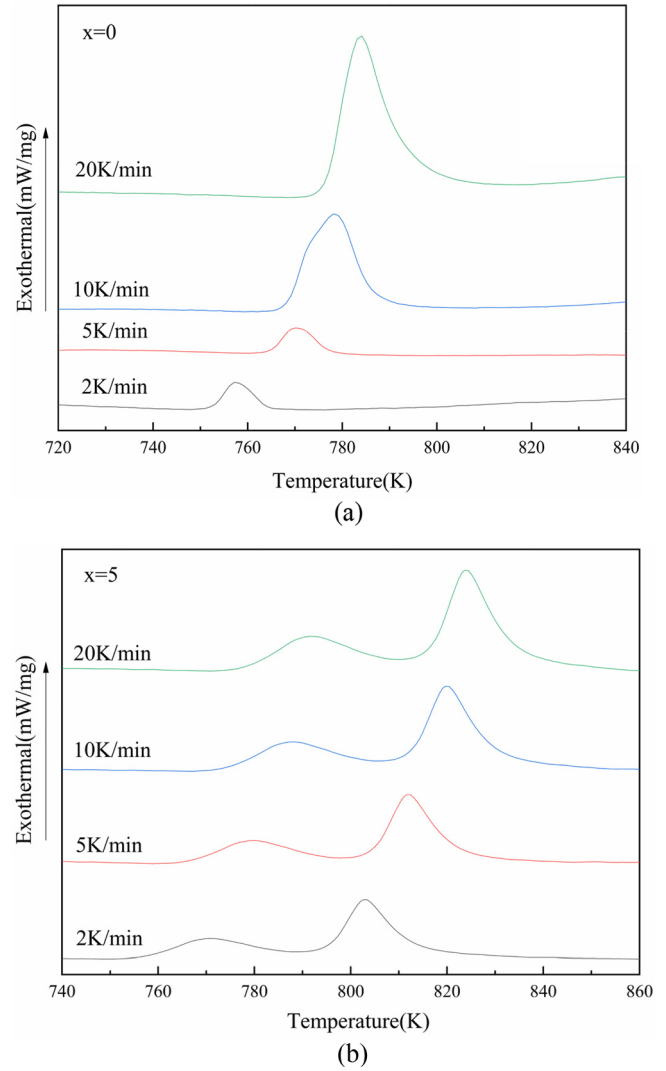


Fig. 5. DSC curves of  $\text{Fe}_{75.5-x}\text{Cr}_4\text{Si}_{3.5}\text{P}_{9.5}\text{B}_{7.5}\text{Mo}_x$  ( $x = 0, 5$ ) alloys obtained by plasma spraying at different heating rates (a)  $x = 0$  (b)  $x = 5$ .

Table 3

Characteristic temperatures from the DSC curves of the  $\text{Fe}_{75.5-x}\text{Cr}_4\text{Si}_{3.5}\text{P}_{9.5}\text{B}_{7.5}\text{Mo}_x$  ( $x = 0, 5$ ) alloys obtained by plasma spraying at different heating rates.

Samples	Heating rates, (K/min)	$T_{x1}$ (K)	$T_{p1}$ (K)	$T_{x2}$ (K)	$T_{p2}$ (K)
$x = 0$	2	752	761		
	5	761	770		
	10	768	778		
	20	772	784		
$x = 5$	2	755	770	791	803
	5	764	779	797	812
	10	772	786	805	818
	20	776	791	810	823

formation of the  $\text{Fe}_3\text{B}$  and  $\text{Fe}_2\text{P}$  phases is drastically retarded, because the stronger bonding between Mo and P, Mo and B can effectively slow down the redistribution of atoms [26]. Second, elements Mo and Fe in the alloy are inclined to form solid solutions, due to their similar electronegativity and atomic size. As a result, the crystallization of  $\text{Fe}_3\text{B}$  and  $\text{Fe}_2\text{P}$  were inhibited to some extent. Moreover, it has been reported that the addition of suitable amount of Mo could lead to sluggish arrangement of Fe-B [10], resulting in the postpone of crystallization process of Fe-B phase.



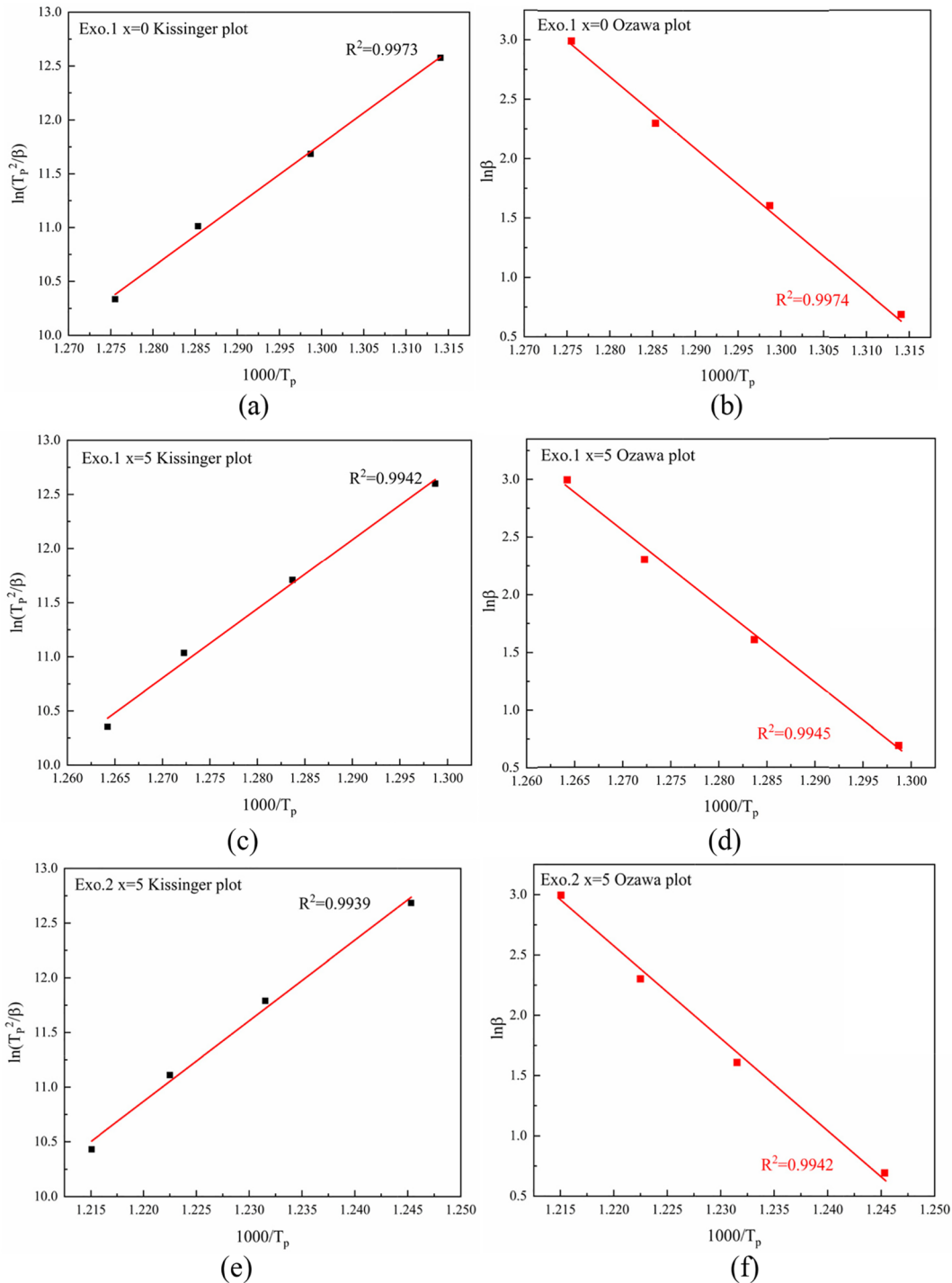


**Fig. 6.** Fitted Kissinger and Ozawa plots of the  $\text{Fe}_{75.5-x}\text{Cr}_4\text{Si}_{3.5}\text{P}_{9.5}\text{B}_{7.5}\text{Mo}_x$  ( $x = 0, 5$ ) alloys obtained by plasma spraying (a) Fitted Kissinger plot of Exo.1 for  $x = 0$  (b) Fitted Ozawa plot of Exo.1 for  $x = 0$  (c) Fitted Kissinger plot of Exo.1 for  $x = 5$  (d) Fitted Ozawa plot of Exo.1 for  $x = 5$  (e) Fitted Kissinger plot of Exo.2 for  $x = 5$  (f) Fitted Ozawa plot of Exo.2 for  $x = 5$ .

**Table 4**

Apparent activation energy of  $\text{Fe}_{75.5-x}\text{Cr}_4\text{Si}_{3.5}\text{P}_{9.5}\text{B}_{7.5}\text{Mo}_x$  ( $x = 0, 5$ ) alloys by Kissinger equation ( $E_a$ ) and Ozawa equation ( $E_a$ ), respectively.

Samples	$E_a$ (kJ/mol)	Kissinger equation	Ozawa equation
$x = 0$	$E_{a1}$	$475.41 \pm 15.50$	$464.30 \pm 15.66$
$x = 5$	$E_{a1}$	$542.39 \pm 16.56$	$528.11 \pm 15.78$
	$E_{a2}$	$545.77 \pm 15.75$	$533.21 \pm 15.02$

#### Crystallization kinetics

Through above analysis,  $\text{Fe}_{75.5-x}\text{Cr}_4\text{Si}_{3.5}\text{P}_{9.5}\text{B}_{7.5}\text{Mo}_x$  ( $x = 0, 5$ ) alloy sheets with a fully amorphous structure can be fabricated by plasma spraying. It is necessary to investigate the crystallization kinetics of first exothermic peak(Exo.1) and second exothermic peak(Exo.2), as shown in Fig. 5. With the increase of heating rate, the initial temperature of crystalline increased. It might be caused by the delay of atom migration at a higher heating rate. In addition, the peak area is also enlarged due to the increased heat released from the grain growth. The apparent

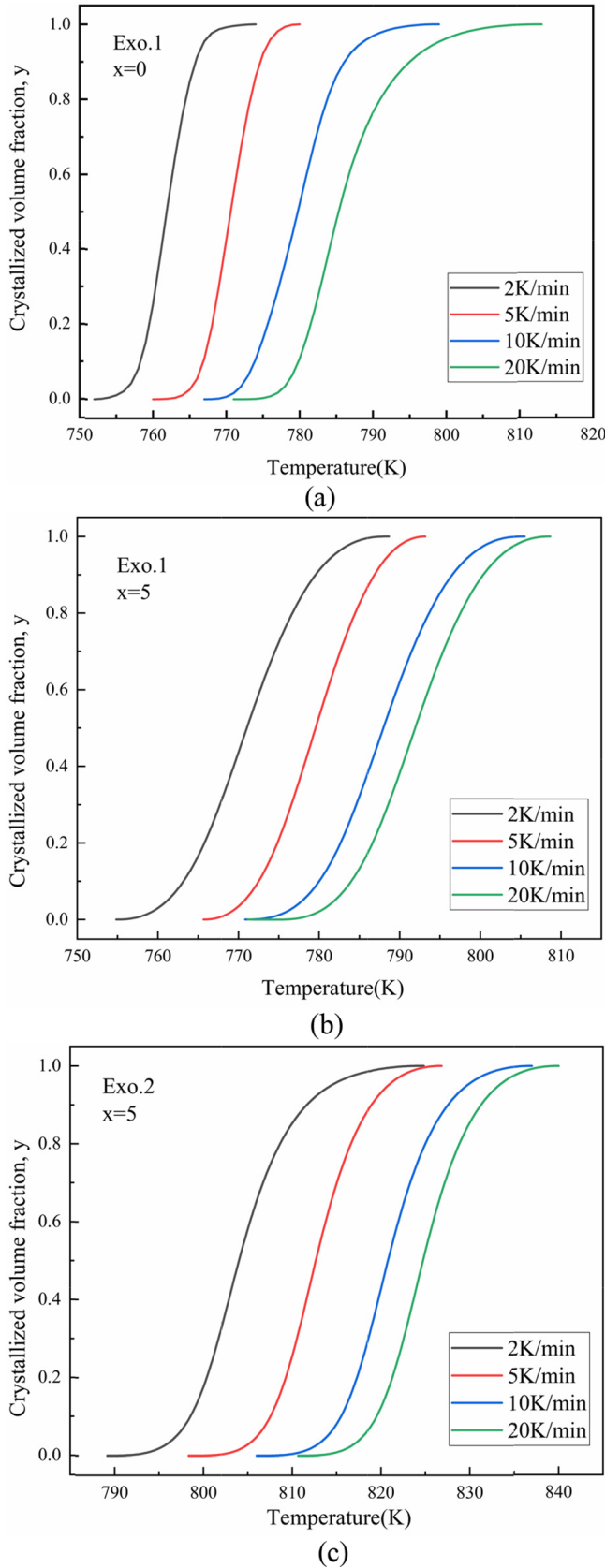


Fig. 7. Relation curves of crystallized volume fraction  $y$  of  $\text{Fe}_{75.5-x}\text{Cr}_4\text{Si}_{3.5}\text{P}_{9.5}\text{B}_{7.5}\text{Mo}_x$  ( $x = 0, 5$ ) and temperature  $T$  at different heating rates (a) Exo.1,  $x = 0$  (b) Exo.1,  $x = 5$  (c) Exo.2,  $x = 5$ .

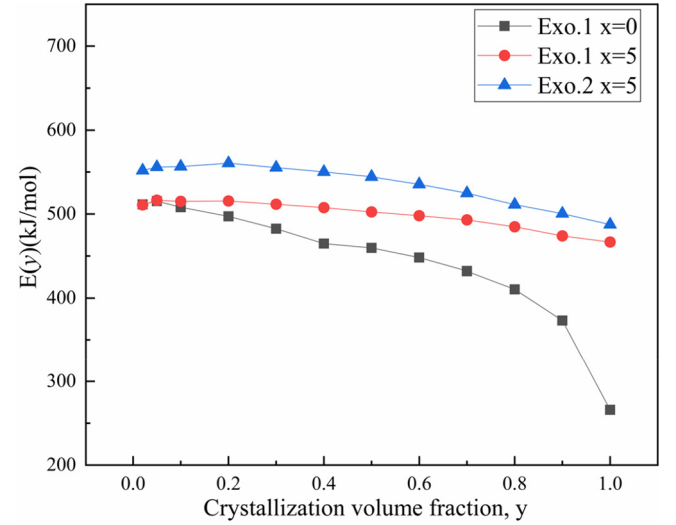


Fig. 8. Plots of  $E_\alpha(y)$  versus crystallization volume fraction  $y$  of  $\text{Fe}_{75.5-x}\text{Cr}_4\text{Si}_{3.5}\text{P}_{9.5}\text{B}_{7.5}\text{Mo}_x$  ( $x = 0, 5$ ).

activation energy ( $E_\alpha$ ) can be fitted according to Kissinger equation (Eq. (1)) [27] and Ozawa equation (Eq.(2)) [28],

$$\ln\left(\frac{\beta}{T_p^2}\right) = \frac{-E_\alpha}{RT_p} + \text{const} \quad (1)$$

$$\ln\beta = \frac{-1.0516E_\alpha}{RT_p} + \text{const} \quad (2)$$

where,  $\beta$  is the heating rate,  $T_p$  is the peak temperature at a certain heating rate,  $E_\alpha$  is the apparent activation energy,  $R$  is the ideal gas constant. Based on the characteristic temperatures of  $\text{Fe}_{75.5-x}\text{Cr}_4\text{Si}_{3.5}\text{P}_{9.5}\text{B}_{7.5}\text{Mo}_x$  ( $x = 0, 5$ ) alloys (Table 3), the square spots were separately plotted by  $\ln(T_p^2/\beta)$  versus  $1000/T_p$  and  $\ln(\beta)$  versus  $1000/T_p$ , as shown in Fig. 6. Subsequently, the curves were fitted according to Eqs. (1) and (2) (Fig. 6), and fitted  $E_\alpha$  of the two exothermic peaks were calculated from the fitting lines, as listed in Table 4. The apparent activation energies ( $E_\alpha$ ) calculated from Kissinger equation and Ozawa equation were close, proving their reasonableness. The  $E_{\alpha 1}$  of as-prepared  $\text{Fe}_{70.5}\text{Cr}_4\text{Si}_{3.5}\text{P}_{9.5}\text{B}_{7.5}\text{Mo}_5$  amorphous alloy was much higher than that of  $\text{Fe}_{75.5}\text{Cr}_4\text{Si}_{3.5}\text{P}_{9.5}\text{B}_{7.5}$  amorphous alloy. This can prove that the thermal stability of  $\text{Fe}_{75.5}\text{Cr}_4\text{Si}_{3.5}\text{P}_{9.5}\text{B}_{7.5}$  amorphous alloy was improved by the addition of 5 at% Mo. The  $E_{\alpha 1}$  value of  $\text{Fe}_{70.5}\text{Cr}_4\text{Si}_{3.5}\text{P}_{9.5}\text{B}_{7.5}\text{Mo}_5$  amorphous alloy is between that of FeCB-MoCrW amorphous alloy ( $453 \text{ kJ}\cdot\text{mol}^{-1}$ ) [22] prepared by copper mold suction casting method and that of FeCrMoBCNb amorphous alloy ( $543 \text{ kJ}\cdot\text{mol}^{-1}$ ) prepared by melt spinning method [29]. It could be attributed to the apparent activation energy of the alloy that is bound up with the cooling rate from the molten state [30]. The actual cooling rate of plasma spraying is between copper mold casting and melt spinning. Therefore, the calculated results are considered to be reasonable. Furthermore,  $E_{\alpha 2}$  of prepared  $\text{Fe}_{70.5}\text{Cr}_4\text{Si}_{3.5}\text{P}_{9.5}\text{B}_{7.5}\text{Mo}_5$  amorphous alloy is slightly higher than  $E_{\alpha 1}$ , indicating that the first step crystallization of the alloy must occur more readily.

It is assumed that the crystallization volume fraction  $y$  is proportional to the released heat during thermal annealing. Thus, the crystallization volume fraction  $y$  can be obtained by measuring the partial area of the exothermic peak at specific temperature divided by the total exothermic peak area. If the released heat of the unit volume alloy is constant during the DSC process, the crystallization volume fraction  $y$  can be calculated by the ratio of the exothermic peak area at a certain temperature  $T$  to the total exothermic peak area. The relation between crystallization volume fraction  $y$  and temperature  $T$  can be obtained at different heating rates [31],

$$\alpha_T = S_T/S \quad (3)$$

where  $S$  is the total exothermic peak area,  $S_T$  is the partial exothermic peak area at a certain temperature  $T$ . The obtained relation curves of crystallization volume fraction and heating temperature  $T$  from Fig. 5 are shown in Fig. 7. A sigmoid shape (S-type) was observed for the curve. This indicates that there is slightly variation in the beginning and at the end of crystallization. The crystallization process might undergo a slow nucleation period and a rapid grain growth.

The relationship between apparent activation energy  $E_a(y)$  and crystallization fraction  $y$  can be obtained according to Kissinger-Akahira-Sunose (KAS) equation [32],

$$\ln\left(\frac{\beta}{T_y^2}\right) = \frac{-E_a(y)}{RT(y)} + \text{const} \quad (4)$$

where  $E_a(y)$  is apparent activation energy corresponding to the certain crystallization fraction  $y$ ,  $T(y)$  is the temperature corresponding to the certain crystallization fraction  $y$ .  $T(y)$  is affected by the heating rate  $\beta$  due to thermodynamic effect. Thus,  $E_a(y)$  at each  $T(y)$  can be obtained by linearly fitting  $\ln(\beta/T_y^2)$  versus  $1/T(y)$ , as shown in Fig. 8. The apparent activation energy  $E_a(y)$  is higher at the initial stage of crystallization ( $y < 0.1$ ), indicating stronger barrier of crystallization process and slow crystallization. It is why the crystallization volume fraction  $y$  (Fig. 6) increased slightly at the initial stage. After that, the crystallization volume fraction  $y$  ( $0.1 < y < 0.9$ ) increased rapidly and the apparent activation energy decreased slowly, indicating a fast crystallization in this process. At the end of the crystallization ( $y > 0.9$ ), the apparent activation energy decreased to a minimum value. The increase rate of crystallization volume fraction changed to be steady, resulting in the decrease of crystallization rate. The apparent activation energy for Exo.1 of prepared  $\text{Fe}_{70.5}\text{Cr}_4\text{Si}_{3.5}\text{P}_{9.5}\text{B}_{7.5}\text{Mo}_5$  amorphous alloy was larger than that of  $\text{Fe}_{75.5}\text{Cr}_4\text{Si}_{3.5}\text{P}_{9.5}\text{B}_{7.5}$  amorphous alloy. This result also proves that the thermal stability of the amorphous alloy was enhanced by the addition of 5 at% Mo. As for prepared  $\text{Fe}_{70.5}\text{Cr}_4\text{Si}_{3.5}\text{P}_{9.5}\text{B}_{7.5}\text{Mo}_5$  amorphous alloy, its apparent activation energy of Exo.2 was larger than that of Exo.1. It indicates that the formation of Fe-B and Fe-P phases in the second step was more difficult.

In conclusion, complete amorphous alloy could be successfully obtained by the introduction of 5 at% Mo in FeCrSiPBMo system through plasma spraying method. And the thermal stability of amorphous alloy was improved. Furthermore, the secondary crystallization precipitation of  $\text{Fe}_3\text{B}$  and  $\text{Fe}_2\text{P}$  was separated from the primary phase, which was beneficial to control the precipitated crystallization phase for preparation of amorphous-nanocrystalline duplex structure. Therefore, the optimal addition amount of Mo is 5 at% in FeCrSiPBMo system for the preparation of amorphous alloy through plasma spraying method and it is favorable to realize the microstructure control of the alloy.

## Conclusion

$\text{Fe}_{75.5-x}\text{Cr}_4\text{Si}_{3.5}\text{P}_{9.5}\text{B}_{7.5}\text{Mo}_x$  ( $x = 0, 1, 3, 5, 7$ ) alloys were successfully fabricated by plasma spraying using industrial raw materials and commercial pure Mo. When the addition contents of Mo were 0 and 5 at %, prepared alloys exhibited a completely characteristic of amorphous phase. As the addition content of Mo was smaller than 5 at%, prepared alloys were composed of  $\alpha$ -Fe crystal phase and amorphous phase. However,  $\alpha$ -Fe(Mo, Si) and  $\text{Fe}_{23}\text{B}_6$  crystalline phases existed in the  $\text{Fe}_{75.5-x}\text{Cr}_4\text{Si}_{3.5}\text{P}_{9.5}\text{B}_{7.5}\text{Mo}_x$  alloy with addition of 7 at% Mo. The addition of 5 at% Mo to  $\text{Fe}_{75.5-x}\text{Cr}_4\text{Si}_{3.5}\text{P}_{9.5}\text{B}_{7.5}\text{Mo}_x$  alloy improved the glass forming ability, changed crystallization behavior and enhanced the thermal stability of the amorphous alloy. The crystallization process changed from one step (amorphous  $\rightarrow \alpha$ -Fe(Si) +  $\text{Fe}_3\text{B}$  +  $\text{Fe}_2\text{P}$ ) to two steps (amorphous  $\rightarrow \alpha$ -Fe(Mo, Si)  $\rightarrow \alpha$ -Fe(Mo, Si) +  $\text{Fe}_3\text{B}$  +  $\text{Fe}_2\text{P}$ ), in which the apparent activation energy of crystallization increased from 475 kJ.mol<sup>-1</sup> to 542 kJ.mol<sup>-1</sup> and 546 kJ.mol<sup>-1</sup>. In addition, the primary precipitation of  $\alpha$ -Fe was inhibited and the secondary

crystallization precipitation of  $\text{Fe}_3\text{B}$  and  $\text{Fe}_2\text{P}$  was separated from the primary phase, favoring the control of the precipitated crystallization phases and promoting the commercial use of the Fe-based amorphous alloys.

## Acknowledgement

This work was financially supported by the Natural Science Foundation of China (51174160), Shaanxi Province Key Laboratory Post-subsidy Program (101-424018016), Scientific Research Program Funded by Shaanxi Provincial Education Department (18JS069, 17JS084) and Natural Science Basic Research Plan in Shaanxi Province of China (2019JQ522).

## Appendix A. Supplementary material

Supplementary data to this article can be found online at <https://doi.org/10.1016/j.rinp.2019.102512>.

## References

- [1] Amiya K, Urata A, Nishiyama N, Inoue A. Fe-B-Si-Nb bulk metallic glasses with high strength above 4000 MPa and distinct plastic elongation. *Mater Trans* 2004;45(4):1214–8.
- [2] Hasiak M, Miglierini M, Łukiewski M, Laszcz A, Bujdoš M. Microstructure soft magnetic properties and applications of amorphous Fe-Co-Si-B-Mo-P alloy. *AIP Adv* 2018;8(5):056116.
- [3] Skulkin NA, Ivanov OA, Mazeeva AK, Kuznetsov PA, Stepanova EA, Blinova OV, et al. Magnetization processes in ribbons of soft magnetic amorphous alloys. *Phys Met Metallogr* 2018;119(2):127–33.
- [4] Han Y, Chang CT, Zhu SL, Inoue A, Louzguine-Luzgin DV, Shalana E, Al-Marzouki F. Fe-based soft magnetic amorphous alloys with high saturation magnetization above 1.5T and high corrosion resistance. *Intermetallics* 2014;54(18):169–75.
- [5] Meng S, Ling H, Qiang L, Zhang J. Development of Fe-based bulk metallic glasses with high saturation magnetization. *Scr Mater* 2014;81(11):24–7.
- [6] Wu Y, Hui XD, Lu ZP, Chen GL, Liang YL. Effects of metalloids elements on the glass-forming ability of Fe-based alloys. *J Alloys Compd* 2009;467(1):187–90.
- [7] Makino A, Kubota T, Makabe M, Chang CT, Inoue A. FeSiBP metallic glasses with high glass-forming ability and excellent magnetic properties. *Mater Sci Eng B* 2008;148(1–3):166–70.
- [8] Shen B, Akiba M, Inoue A. Effect of Cr addition on the glass-forming ability, magnetic properties, and corrosion resistance in FeMoGaPCBSi bulk glassy alloys. *J Appl Phys* 2006;100(4):043523.
- [9] Shen J, Chen Q, Sun J, Fan H, Wang G. Exceptionally high glass-forming ability of an FeCoCrMoCBy alloy. *Appl Phys Lett* 2005;86(15):151907.
- [10] Li HX, Kim KB, Yi S. Enhanced glass-forming ability of Fe-based bulk metallic glasses prepared using hot metal and commercial raw materials through the optimization of Mo content. *Scr Mater* 2007;56(12):1035–8.
- [11] Li H, Yi S, Sohn HS. Fe-based bulk metallic glasses  $\text{Fe}_{73.8-x}\text{Cr}_7.0\text{Si}_{3.5}\text{B}_p\text{P}_{9.6}\text{Cr}_{2.1}\text{Mo}_{2.0}\text{Al}_{2.0}$  ( $x = 3-9$ ) prepared using hot metal and industrial raw materials. *J Mater Res* 2007;22(1):164–8.
- [12] Li HX, Wang SL, Yi S, Jiao ZB, Lu ZP, Wu Y. Glass formation and magnetic properties of Fe-Cr-Si-B-P-(Cr-Al-Co) bulk metallic glasses fabricated using industrial raw materials. *J Magn Magn Mater* 2009;321(18):2833–7.
- [13] Wang SL, Li HX, Zhang XF, Yi S. Effects of Cr contents in Fe-based bulk metallic glasses on the glass forming ability and the corrosion resistance. *Mater Chem Phys* 2009;113(2–3):878–83.
- [14] Guo W, Wu Y, Zhang J, Hong S, Li GY, Ying GB, et al. Fabrication and characterization of thermal-sprayed Fe-based amorphous/nanocrystalline composite coatings: an overview. *J Therm Spray Technol* 2014;23(7):1157–80.
- [15] Zhou Z, Wang L, He DY, Wang FC, Liu YB. Microstructure and electrochemical behavior of Fe-based amorphous metallic coatings fabricated by atmospheric plasma spraying. *J Therm Spray Technol* 2011;20(1–2):344–50.
- [16] WuYP Lin PH, Xie GZ, Hu JH, Cao M. Formation of amorphous and nanocrystalline phases in high velocity oxy-fuel thermally sprayed a Fe-Cr-Si-B-Mn alloy. *Mat Sci Eng A-Struct* 2006;430(1–2):34–9.
- [17] Zhang J, Shen B, Zhang Z. Crystallization behaviors of FeSiBPmo bulk metallic glasses. *J Non-Cryst Solids* 2013;360:31–5.
- [18] Takeuchi A, Inoue A. Classification of bulk metallic glasses by atomic size difference, heat of mixing and period of constituent elements and its application to characterization of the main alloying element. *Mater Trans* 2005;46(12):2817–29.
- [19] Li K, Xue D. Estimation of electronegativity values of elements in different valence states. *J Phys Chem A* 2006;110(39):11332–7.
- [20] Lu ZP, Liu CT, Dong YD. Effects of atomic bonding nature and size mismatch on thermal stability and glass-forming ability of bulk metallic glasses. *J Non-Cryst Solids* 2004;341(1–3):93–100.
- [21] Guo S, Liu CT. Phase stability in high entropy alloys: formation of solid-solution phase or amorphous phase. *Prog Nat Sci Mater Int* 2011;21:433–46.
- [22] Yang X, Ma X, Li Q, Guo S. The effect of Mo on the glass forming ability, mechanical

- and magnetic properties of FePC ternary bulk metallic glasses. *J Alloys Compd* 2013;554:446–9.
- [23] Li X, Qin C, Kato H, Makino A, Inoue A. Mo microalloying effect on the glass-forming ability, magnetic, mechanical and corrosion properties of  $(\text{Fe}_{0.76}\text{Si}_{0.096}\text{B}_{0.084}\text{P}_{0.06})_{100-x}\text{Mo}_x$  bulk glassy alloys. *J Alloys Compd* 2011;509(29):7688–91.
- [24] Khalifa HE, Cheney JL, Vecchio KS. Effect of Mo-Fe substitution on glass forming ability, thermal stability, and hardness of Fe-C-B-Mo-Cr-W bulk amorphous alloys. *Mater Sci Eng A* 2008;490(1–2):221–8.
- [25] Takahara Y, Narita N. Classification of crystallization process of Fe-B-Si amorphous alloys by electrical resistivity and calorimetric measurements. *Mater Trans JIM* 2000;41(8):1077–81.
- [26] Jiao ZB, Li HX, Wu Y, Gao JN, Wang SL, Yi SH, Lu ZP. Effects of Mo additions on the glass-forming ability and magnetic properties of bulk amorphous Fe-C-Si-BP-Mo alloys science China physics. *Mech. Astronomy* 2010;53(3):430–4.
- [27] Sánchez-Jiménez PE, Criado JM, Pérez-Maqueda LA. Kissinger kinetic analysis of data obtained under different heating schedules. *J Therm Anal Calorim* 2008;94(2):427–32.
- [28] Zhu M, Li JJ, Yao LJ, Jian ZY, Chang FE, Yang GC. Non-isothermal crystallization kinetics and fragility of  $(\text{Cu}_{46}\text{Zr}_{47}\text{Al}_7)_{97}\text{Ti}_3$  bulk metallic glass investigated by differential scanning calorimetry. *Thermochim Acta* 2013;565:132–6.
- [29] Ahmadi S, Shahverdi HR, Saremi SS. Effects of Nb alloying on nano-crystallization kinetics of  $\text{Fe}_{85-x}\text{Cr}_{18}\text{Mo}_7\text{B}_{16}\text{C}_4\text{Nb}_x$  ( $x=0,3$ ) bulk amorphous alloys. *J Mater Sci Technol* 2011;27(8):735–40.
- [30] Waniuk TA, Schroers J, Johnson WL. Critical cooling rate and thermal stability of Zr-Ti-Cu-Ni-Be alloys. *Appl Phys Lett* 2001;78(9):1213–5.
- [31] Han SC, Peng P, Zheng CX, Liu JS, Xu ZY, Liu RS. Measurement and control of the crystallinity of amorphous alloy during crystallization by DSC. *J Hunan University (Natural Sci.)* 2003;30(6):41–4. (in Chinese).
- [32] Minić DM, Adnadević B. Mechanism and kinetics of crystallization of  $\alpha$ -Fe in amorphous  $\text{Fe}_{81}\text{B}_{13}\text{Si}_4\text{C}_2$  alloy. *Thermochim Acta* 2008;474(1–2):41–6.